Proceedings of the ASME/BATH 2021
Symposium on Fluid Power and Motion Control
FPMC2021
October 19-21, 2021, Virtual, Online

FPMC2021- 68832

EFFICIENT CONTROL OF A SWITCHED INERTANCE HYDRAULIC CONVERTER WITH A TIME-VARYING LOAD

Chenggang Yuan
cy466@bath.ac.uk
University of Bath
Bath, United Kingdom

Andrew Plummer
arp23@bath.ac.uk
University of Bath
Bath, United Kingdom

Min Pan*
mp351@bath.ac.uk
University of Bath
Bath, United Kingdom

ABSTRACT

Switched inertance hydraulic converters (SIHC) are new digital hydraulic devices which provide an alternative to conventional proportional or servo valve-controlled systems in hydraulic fluid power. SIHCs can adjust and control flow and pressure by means of using digital control signals that do not rely on throttling the flow and dissipation of power, and provide hydraulic systems with high-energy efficiency, good controllability, and insensitivity to contamination. A flow booster is one configuration of SIHCs which can deliver more flow than the supply flow. In this article, the loading effects of SIHCs are investigated by applying a time-varying load on the flow booster. A control system consisting of a PI controller and a switching frequency optimizer was designed to operate a flow booster at its optimal switching frequencies and switching ratios to maximize system efficiency when the load varies. Simulated results showed that the flow booster with the proposed controller has very good dynamic response and can be operated at an average efficiency of 70% with a time-varying load. Compared with only using a PI controller, the proposed controller can improve the overall efficiency by up to 20%. As time-varying loading conditions are commonly found in hydraulic applications, this work constitutes an important contribution to the design and development of high-efficiency SIHCs.

Keywords: Digital hydraulics; Switched inertance hydraulic converters; Hydraulic efficiency; Time-varying load

1. INTRODUCTION

Digital hydraulics is a new technology providing an alternative to conventional valve-throttling systems, which promises hydraulic systems with high-energy efficiency, good controllability and insensitivity to contamination [1-4]. The switched inertance hydraulic converter (SIHC) concept is a sub-domain of digital hydraulics, which is analogous to the electrical buck converter [4-6]. **FIGURE 1(a)** shows a classic three-port SIHC in a flow booster configuration [9], which is analogous to the electrical buck converter, as shown in **FIGURE 1(b)** [10]. The flow booster consists of a three-port high-speed switching valve, an inertance tube, and an accumulator, acting as the switch, inductor, and capacitor of an electrical buck converter. A 3/2-way high-speed switching valve is connected to the high-pressure supply (HP) and the low-pressure supply (LP). When the flow booster operates, the high-speed switching valve switches alternately between the HP and LP supplies at the operating switching frequency. When the valve connects to the HP line, the high-velocity fluid passes from the HP to the load; when the valve switches from the HP to the LP port, the momentum of the fluid along the inertance tube draws the continuous flow Q_{LP} from the LP supply to the load despite the adverse pressure gradient. As long as the switching time of the valve is short, the reduction in delivery flow $Q_{DELIVERY}$ will be very small, and the average delivery flow can be boosted, i.e. it will be significantly higher than the supply flow Q_{HP}, but delivered at a lower pressure. The use of the flow booster can significantly improve energy efficiency of hydraulic fluid power systems. The flow booster combined with a fixed-displacement pump is functionally equivalent to a variable displacement pump which can also achieve high energy efficiency but with additional bulky structure, sluggish response and higher costs compared with the SIHCs [7, 8]. SIHCs also allow programmable control by adjusting the switching ratio with pulse-width-modulated signals.

The concept, configurations, and exploitation of SIHCs have been explored by a number of research groups in the last decade [9-22]. Significant progress has been achieved in the aspects of analytical modelling [10, 21], experimental investigations [9-11, 20-22] and real-life applications [12-19]. These have been summarised in comprehensive reviews with achievements, perspectives, and challenges of this new digital switched hydraulics field [3-5].

This article reports the development of a new control system for a three-port flow booster with a time-varying load. The control system is designed by integrating a PI controller and a switching frequency optimizer which is based on minimizing the wave propagation effect along the inertance tube. The velocity and force control are conducted in simulation to evaluate the performance of the proposed controller and the loading effects on the flow booster. Simulated results show that the flow booster using the proposed controller can effectively adapt to the time-varying load and operate at an average efficiency of 70%, which is improved by up to 20% compared with just using a PI controller. The load stiffness effects on the flow booster are also investigated by using different springs. It is found that the efficiency of the flow booster with the proposed controller is up to 17% higher with a stiffer spring because the flow booster is operated at higher switching ratios to overcome larger spring force in velocity control. While in force control, the maximum efficiency improvement of the flow booster achieves 10% with a stiffer spring due to less damping.

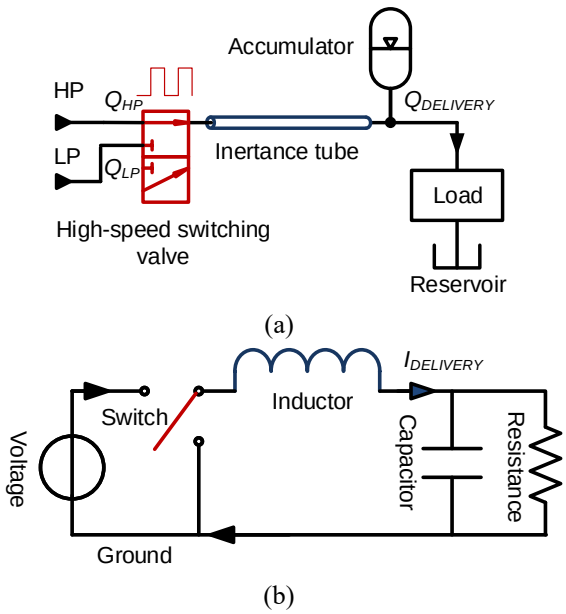

FIGURE 1: (a) SCHEMATIC OF A THREE-PORT FLOW BOOSTER [9]; (b) SCHEMATIC OF AN ELECTRICAL BUCK CONVERTER [10]

2. THE NUMERICAL MODEL OF A FLOW BOOSTER

The numerical model of a flow booster is developed in MATLAB/Simulink. The model consists of a 3/2-way high-speed switching valve, an inertance tube and an accumulator, as shown in **FIGURE 2**. The valve is modelled by the HP and LP orifices using the standard valve orifice equation (1), integrating with the valve switching transition characteristics.

$$q = C_q A \sqrt{\frac{2|\Delta p|}{\rho}} \operatorname{sgn} \Delta p \qquad (1)$$

where q is the flow rate through the orifice, C_q is the flow coefficient, A is the orifice area, Δp is the pressure difference between the inlet and outlet of the orifice, and ρ is the density of the fluid. A small compressible volume (5 cm^3) is used between the switching valve and the inertance tube to represent the volume of the valve. This is modelled by equation (2):

$$p = \int \frac{q}{V} B dt \qquad (2)$$

where p is the valve output pressure, V is the fluid volume, B is the bulk modulus of the fluid and q is the difference in volume flow rate between inlet and outlet flows.

The Transmission Line Method (TLM) is used to model the inertance tube. The TLM model was developed by Krus *et al* [23] and modified by Johnston [24] to include unsteady or frequency-dependent friction, which can accurately and effectively represent wave propagation and laminar friction over a wide frequency range. The details of the model can be found in [24].

In addition, a large volume of 0.02 m^3 is used to model the downstream accumulator in order to reduce delivery pressure pulsation.

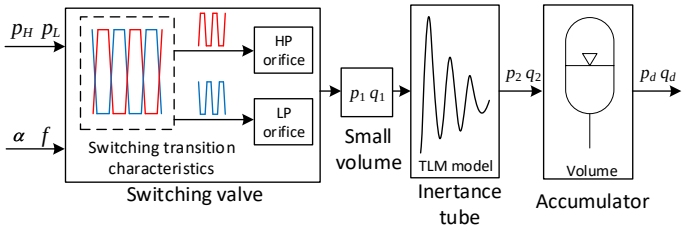

FIGURE 2: SCHEMATIC DIAGRAM OF THE NUMERICAL MODEL OF A FLOW BOOSTER

3. THE TIME-VARYING LOAD

The flow booster is used to drive a time-varying load which consists of a single-ended cylinder actuating a mass-spring-damper system, as shown in **FIGURE 3**. The delivery flow of the flow booster $Q_{DELIVERY}$ is supplied to the piston chamber of the cylinder while the annulus chamber connects to the tank. The mass is attached to the cylinder rod and moves against the spring and the damper. Thus, the required load force and pressure will vary according to the demand motion.

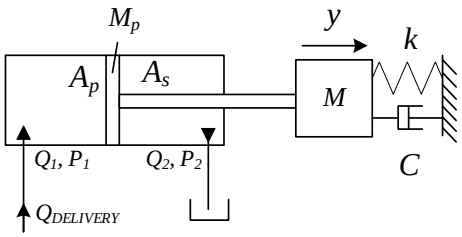

FIGURE 3: SCHEMATIC DIAGRAM OF THE TIME-VARYING LOAD

The force balance of the loading system is given by equation (3):

$$(P_1 A_p - P_2 A_s) = ky + C\dot{y} + (M_p + M)\ddot{y} \qquad (3)$$

where P_1 and P_2 are the pressures of the piston and annulus

chambers of the cylinder, A_p and A_s are the piston and annulus areas, M_p is the piston mass, M is the load mass, k is the spring constant, C is the damper constant, and $y, \dot{y}$, and $\ddot{y}$ are the position, velocity, and acceleration of the mass.

The piston pressure P_1 and the annulus pressure P_2 are given by equation (4):

$$P_1 = \int (Q_1 - A_p \dot{y}) \frac{B}{V_1} dt$$
$$P_2 = \int -(Q_2 - A_s \dot{y}) \frac{B}{V_2} dt \quad (4)$$

where Q_1 and Q_2 are the flow rates to the piston and annulus chambers of the cylinder, V_1 and V_2 are the volumes of the piston and annulus chambers, B is the bulk modulus of the fluid.

4. CONTROL SYSTEM DESIGN

Optimized switching frequencies and ratios for SIHCs based on minimizing wave propagation effect at the switching valve were proposed in [20] and experimentally validated in [21] and [22]. With the optimal switching frequencies and ratios, the wave delay time is equal to the duration of the high-pressure supply (α < 0.5) or low-pressure supply (α > 0.5). The pulsations from the switching are synchronized with the pulsations due to the wave propagation; thus, the wave propagation effect is minimized. This reduces the pressure ripple and flow loss and improves system efficiency. The optimal frequency is defined as [20]:

$$f = \begin{cases} \dfrac{\alpha c}{2L} & 0 \le \alpha \le 0.5 \\ \dfrac{(1-\alpha)c}{2L} & 0.5 < \alpha \le 1 \end{cases} \quad (5)$$

where f is the switching frequency, α is the switching ratio, c is the speed of sound, and L is the length of the inertance tube.

A control system is designed to achieve high efficiency by integrating a PI controller with a switching frequency optimizer to operate the flow booster at its optimal switching frequencies and ratios. The schematic diagram of the control system is shown in **FIGURE 4**.

The plant output to be controlled might be the actuator position, velocity or force. Based on the demand and feedback signal, the PI controller outputs the switching ratio α to the switching frequency optimizer, which calculates the optimal switching frequency f_{opt} using Equation (5) and uses it as the output frequency f to the plant. It was found that when the switching frequency changes continuously, the switching ratio shows large spikes and oscillations. This is undesired for the system, which needs to be further investigated. To reduce the unexpected spikes, a trigger and a switch are designed within the switching frequency optimizer as shown in **FIGURE 4**. The current switching frequency of the plant f is compared with the calculated optimal frequency f_{opt}. Only when the frequency difference between f and f_{opt} reaches the threshold value f_t, the new switching frequency f_{new} updates as the optimal frequency f_{opt}, otherwise it remains unchanged as the current switching frequency f. In this case, the switching frequency changes in the step of f_t to avoid continuous disturbance to the switching ratio.

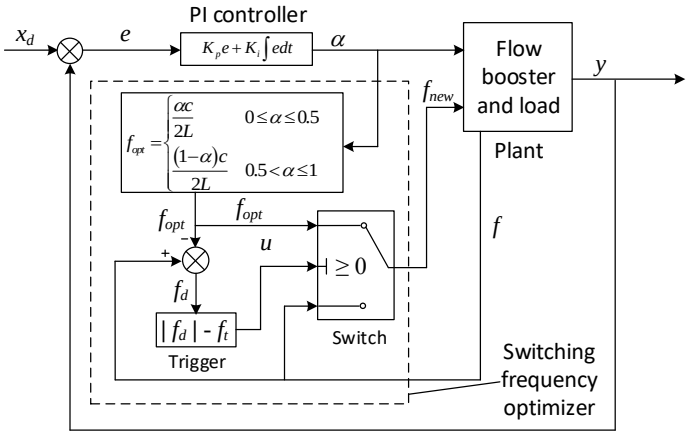

FIGURE 4: THE CONTROL SYSTEM CONSISTING OF THE PI CONTROLLER AND THE SWITCHING FREQUENCY OPTIMIZER

5. RESULTS AND DISCUSSION

The control of the velocity (velocity control) and the force (force control) of the single-ended cylinder in the time-varying load are investigated to evaluate the performance of the proposed controller and the load effects on the flow booster. The parameters listed in **Table 1** are used in simulations.

Table 1. PARAMETERS FOR SIMULATION MODEL

Parameters	Value (unit)
Fluid viscosity v	30 cSt
Fluid density ρ	870 kg/m3
Fluid bulk modulus B	1.6×10^9 Pa
Speed of sound c	1300 m/s
High-supply pressure p_H	90 bar
Low-supply pressure p_L	30 bar
Inertance tube length L	1.66 m
Cylinder piston mass M_p	11.2 kg
Load mass M	50 kg
Load damping constant C	30 kN/(m/s)
Load spring stiffness k	5 kN/m
Threshold value of frequency change f_t	20 Hz

5.1 Velocity control

The simulated results for velocity control achieved by using the proposed controller (optimized) are presented in **FIGURE 5-8**. For comparison, the results of using a PI controller with a fixed switching frequency of 200Hz (non-optimized) are also plotted.

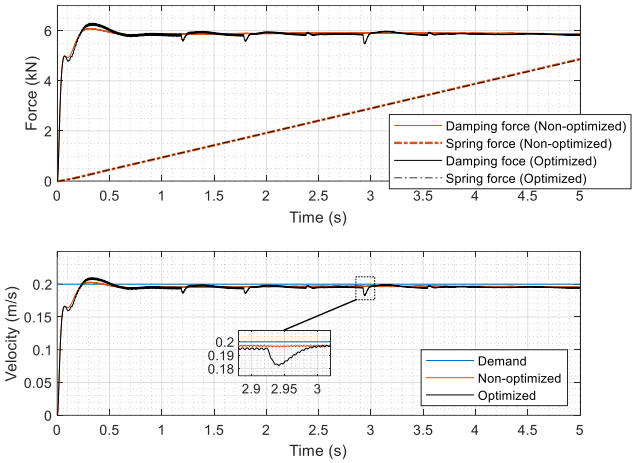

FIGURE 5: THE DAMPING FORCES, THE SPRING FORCES AND THE VELOCITY RESPONSES IN VELOCITY CONTROL

FIGURE 5 shows the damping forces, spring forces and velocity responses for a step change in demand. The time-varying load effects represented by the damper and the spring can be seen from the damping forces and the spring forces. With the step demand velocity, the damping force builds up quickly within 0.3 s then remains nearly constant while the spring force keeps increasing linearly with time. In this case, the spring effect is the dominant load effect. There is no obvious difference between the optimized and non-optimized results in terms of the damping force and the spring force except for the peaks caused by the frequency changes, which shows that the proposed controller has little effect on the system dynamics. The peaks could be caused by the valve transition dynamics when the switching frequency changes. As shown in **FIGURE 5**, good velocity responses are achieved under the time-varying load, with a response time of less than 0.2 s and a steady-state error of less than 3%. Additional peaks can also be observed in the velocity of the optimized result due to the frequency changes. The maximum velocity deviation caused by the peaks is about 5% within a time frame of 0.06 s, as shown in the detailed plot.

The switching ratios, switching frequencies and efficiencies of the flow booster in velocity control are plotted in **FIGURE 6**. The switching ratios of the flow booster increase quickly to 20% within 0.2 s to deliver high pressure to provide acceleration and damping forces, and then keep increasing to overcome the increasing spring force. Accordingly, the optimized switching frequency increases from 40 Hz to 180 Hz in steps of 20 Hz. The efficiency of the flow booster increases following the trend of the increase of the switching ratio. The system efficiency η is calculated as [10]:

$$\eta = \frac{(p_H\alpha + p_L(1-\alpha))q_m - q_m^2 R}{(p_H\alpha + p_L(1-\alpha))q_m + q_{loss}(p_H - p_L)} \qquad (6)$$

where p_H and p_L are the supply pressures, α is the switching ratio, q_m is the mean delivery flow rate, R is the overall system resistance, q_{loss} is the flow loss. The efficiency with optimized switching frequencies is significantly improved (up to 20%) compared with the non-optimized result

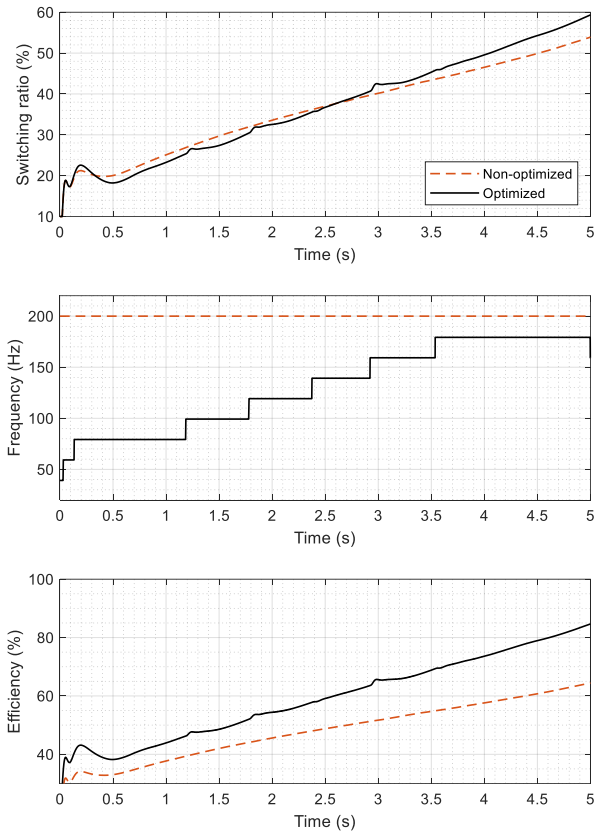

FIGURE 6: THE SWITCHING RATIOS, SWITCHING FREQUENCIES AND EFFICIENCIES OF THE FLOW BOOSTER IN VELOCITY CONTROL

The delivery pressures and the delivery flows of the flow booster are shown in **FIGURE 7**. The delivery pressures of the flow booster rise quickly to about 32 bar within 0.4 s at the beginning to overcome the damping force and then keep increasing linearly to resist the increasing spring force, which shows the time-varying load effects on the flow booster. The pressure peak caused by the frequency change can be clearly seen from the detailed plot. The other detailed plot shows the reduced pressure ripple (up to 50% reduction of peak to peak value) with optimized frequencies due to the improvement of the wave propagation effects, showing the efficacy of the proposed controller. The delivery flows of the flow booster show a quick settling time of 0.5 s with some fluctuations at the beginning. The detailed plots show the reduction of the flow ripple (up to 23%) at the optimized switching frequency and the flow peak due to the frequency change.

The effects of the load stiffness on the flow booster are investigated by simulating the velocity control with different springs in the load. The delivery pressures and efficiencies of the flow booster using the proposed controller are presented in **FIGURE 8** to show the load stiffness effect. The delivery pressure increases more steeply with the stiffer spring because the spring force increases more quickly while the damping force is nearly constant with the constant velocity demand. The

efficiencies of the flow booster in **FIGURE 8** show that the flow booster against the load with a stiffer spring achieves higher delivery pressure (maximum of 54 bar at 5 kN/m and 44 bar at 3 kN/m) and higher efficiency (maximum of 85% at 5 kN/m and 68% at 3 kN/m). This is because it is operated at higher switching ratios to deliver higher pressure to overcome the larger spring force. It can be concluded that the flow booster with the proposed controller can adapt to the load with different stiffnesses and achieve up to 17% efficiency improvement with a stiffer load in velocity control.

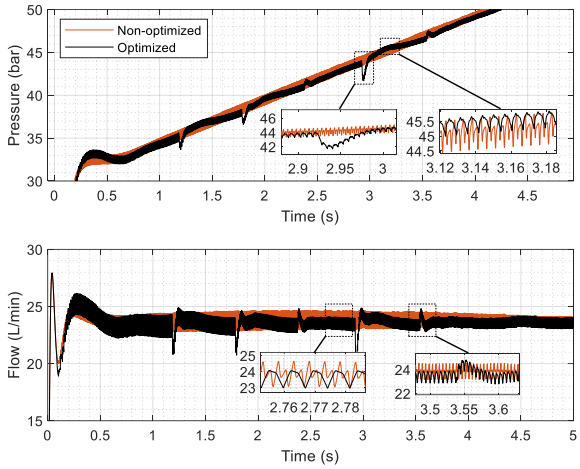

FIGURE 7: THE DELIVERY PRESSURES AND THE DELIVERY FLOWS OF THE FLOW BOOSTER IN VELOCITY CONTROL

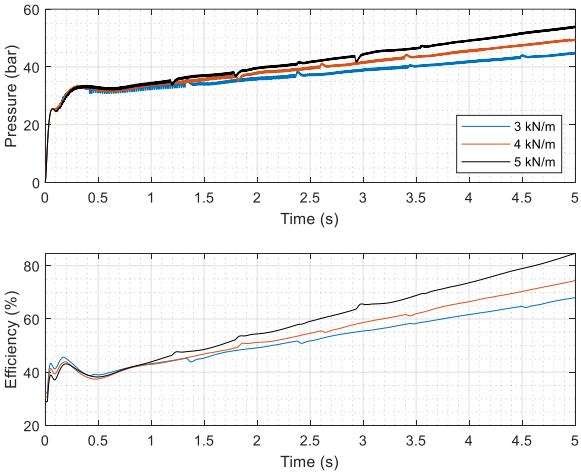

FIGURE 8: THE DELIVERY PRESSURES AND THE EFFICIENCIES OF THE FLOW BOOSTER WITH DIFFERENT SPRINGS IN VELOCITY CONTROL

5.2 Force control

Force control has also been investigated. Simulated results for a step demand achieved by using the proposed controller with the optimized frequency (optimized) and the baseline PI controller with a constant frequency of 200Hz (non-optimized) are presented and compared in **FIGURE 9-12**.

FIGURE 9 shows the time-varying damping forces, spring forces, and force responses in force control using both controllers. The damping forces rise quickly to 12 kN within 0.4 s and gradually decrease with the increasing spring force. This is because the mass accelerates at the beginning to build up the damping force to achieve the demand force in force control, and then it decelerates gradually with the increase of the spring force to maintain the constant demand force of the mass-spring-damper system. Finally, the mass will stop when the spring force is balanced with the demand force and the damping force will become zero. Different to velocity control, both the damper and spring have significant time-varying load effects in force control. Good force responses are achieved in resisting the time-varying load, with a rising time of less than 0.5 s and a steady-state error of less than 1%. There is little difference except for the peaks caused by the frequency changes. The maximum force deviation caused by the peaks is about 2% within 0.06 s, as shown in the detailed plot.

The switching ratios, switching frequencies and efficiencies of the flow booster in force control are presented in **FIGURE 10**. The switching ratios of the flow booster increase to about 87% within 0.2 s at the beginning to deliver high pressure to resist the large damping force, and then keep decreasing to about 60% to maintain the constant demand force of the mass-spring-damper system. As a result, the optimized frequency increases rapidly to 180 Hz within 0.05s before dropping to 60 Hz at 0.2 s and then gradually increases back to 140 Hz at 4.1 s. The efficiencies of the flow booster show a similar trend as the switching ratio, increasing to the peak values (82% and 72%) and decreasing to the minimum values (62% and 55%). The efficiency of the flow booster with optimized frequencies has been significantly improved (up to 10%) compared with the non-optimized result, showing the advantage of the proposed controller.

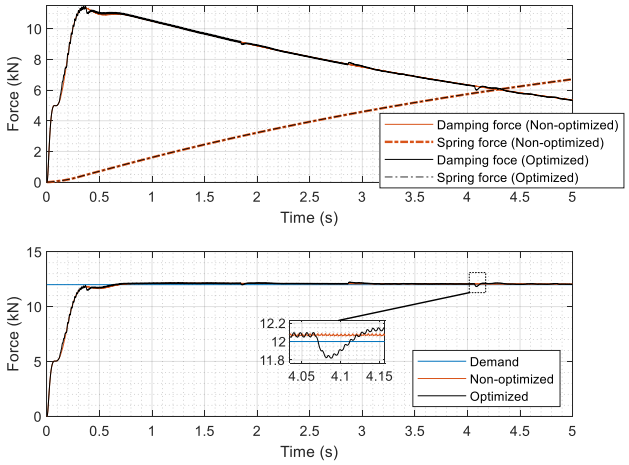

FIGURE 9: THE DAMPING FORCES, THE SPRING FORCES AND THE FORCE RESPONSES IN FORCE CONTROL

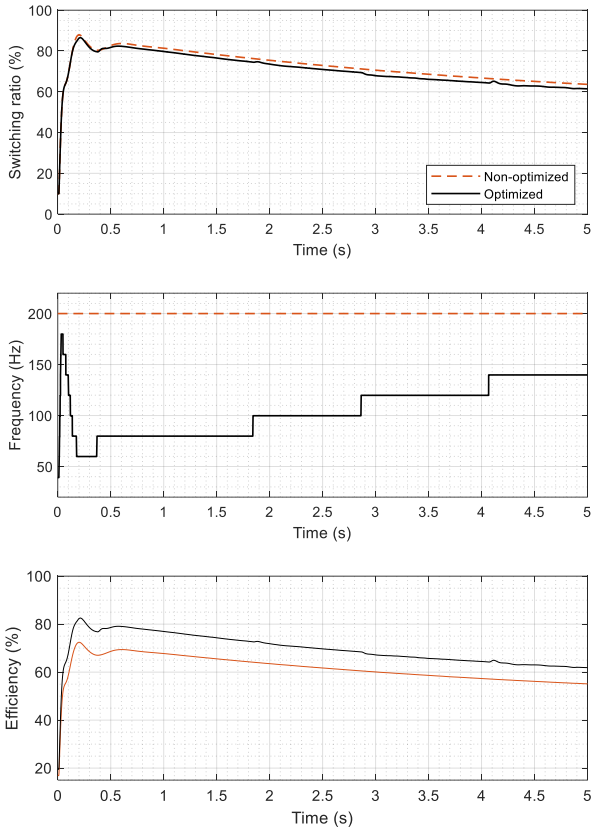

FIGURE 10: THE SWITCHING RATIOS, SWITCHING FREQUENCIES AND EFFICIENCIES OF THE FLOW BOOSTER IN FORCE CONTROL

FIGURE 11 shows the delivery pressures and the delivery flows of the flow booster in force control using both controllers. The delivery pressures rise quickly to 60 bar in 0.4 s and then are nearly constant to maintain the demand force while the delivery flows quickly increase to the maximum of 48 L/min at 0.3 s and then gradually decrease to 20 L/min at 5 s. This is because the mass accelerates at the beginning to build up the damping force and then gradually decelerates before it stops. The peaks caused by the frequency change in the delivery flows and the delivery pressures can be seen in the detailed plots. It can also be seen from the detailed plots that the optimized results of the delivery flow and the delivery pressure show the reduced pressure ripple (40%) and the flow ripple (17%) due to the improved wave propagation effects. However, the reductions are not obvious for the time range of 0.2-1.9 s because the switching frequencies are below 100 Hz and the ripples are large due to the long switching time.

The force control with different springs used in the load is simulated to investigate the load stiffness effects on the flow booster. As can be seen from the delivery flows and efficiencies of the flow booster in **FIGURE 12**, the delivery flow of using a spring of 5 kN/m is reduced by up to 10 L/min and the efficiency is improved by up to 10%, compared with the results of 3 kN/m. This is because the stroke needed for the mass to stop is less due to the higher stiffness and the velocity (related to the delivery flow) in this case is smaller within the same time frame. The lower velocity reduces the energy consumed by the damper and improves the efficiency of the flow booster.

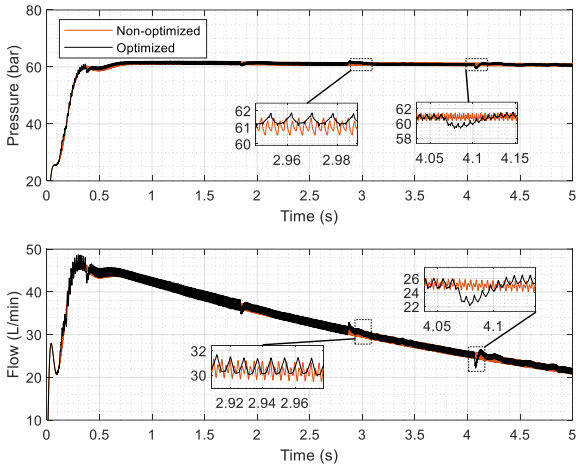

FIGURE 11: THE DELIVERY PRESSURES AND THE DELIVERY FLOWS OF THE FLOW BOOSTER IN FORCE CONTROL

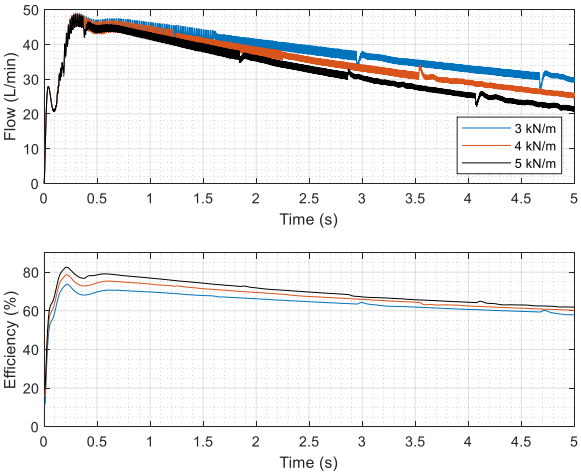

FIGURE 12: THE DELIVERY FLOWS AND THE EFFICIENCIES OF THE FLOW BOOSTER WITH DIFFERENT SPRINGS IN FORCE CONTROL

6. CONCLUSION

A numerical model of the flow booster to drive a time-varying load is created, and a controller consisting of a PI controller and a switching frequency optimizer is developed. The switching frequency optimizer includes a deadband to prevent undesired disturbances due to the real-time change of the switching frequency. Velocity control and force control are investigated in simulation using the proposed controller, compared with using a PI controller. The results show the system has good dynamic response for both velocity response (rising time < 0.2 s and steady-state error < 3%) and force response (rising time < 0.5 s and steady-state error < 1%). The flow booster with the proposed controller can operate at the optimal

frequencies, which has shown significant efficiency improvement (up to 20% in velocity control and 10% in force control). The flow and pressure ripples have been reduced due to improved wave propagation effects resulting from using the optimal frequencies. The load stiffness effects on the flow booster are investigated by using different springs. In the velocity control, the flow booster shows higher efficiency with stiffer springs because it is operated at higher switching ratios. The efficiency improvement has achieved up to 17% by using a spring of 5 kN/m compared with that of using a spring of 3 kN/m. While in the force control, the efficiency of the flow booster is higher when driving stiffer springs due to less damping. In this case, the efficiency of the flow booster driving a spring of 5 kN/m is improved by up to 10% compared to using a spring of 3kN/m. In the future, the disturbances such as the peaks introduced by the frequency change using the proposed controller will be further studied. Experiments will be conducted to validate the simulation results. Loading systems such as hydraulic motors will also be used to explore the effect of other load characteristics such as large inertias on the SIHCs.

ACKNOWLEDGEMENTS

This research was funded by the RAEng/The Leverhulme Trust Senior Research Fellowship, UK, grant number LTSRF1819\15\16, the RAEng Proof-of-Concept Award PoC1920/15. Chenggang Yuan thanks the support from the China Scholarship Council PhD studentship (201706150102).

REFERENCES

[1] Scheidl, R., Linjama, M. and Schmidt, S., 2012, "Is the future of fluid power digital?," *Proceedings of the Institution of Mechanical Engineers, Part I: Journal of Systems and Control Engineering*, 226(6), pp. 721-723.

[2] Yang, H.Y. and Pan, M., 2015, "Engineering research in fluid power: a review," *Journal of Zhejiang University-Science A*, 16(6), pp. 427-442.

[3] Pan, M., and Plummer, A., 2018, "Digital switched hydraulics," *Frontiers of Mechanical Engineering*, 13(2), pp. 225-231.

[4] Yuan, C., Pan, M., and Plummer, A., 2018, "A review of switched inertance hydraulic converter technology," Proceedings of the BATH/ASME 2018 Symposium on Fluid Power and Motion Control, Bath, UK, September 12-14, 2018, Paper No. FPMC2018-8829.

[5] Yuan, C., Pan, M. and Plummer, A., 2020, "A review of switched inertance hydraulic converter technology," *Journal of Dynamic Systems, Measurement, and Control*, 142(5): 050801.

[6] Brandstetter, R., Deubel, T., Scheidl, R., Winkler, B. and Zeman, K., 2017, "Digital hydraulics and "Industrie 4.0"," *Proceedings of the Institution of Mechanical Engineers, Part I: Journal of Systems and Control Engineering*, 231(2), pp. 82-93.

[7] Li, P.Y., Li, C.Y. and Chase, T.R., 2005, "Software enabled variable displacement pumps," ASME International Mechanical Engineering Congress and Exposition, Orlando, Florida, USA, November 5-11, 2005, Vol. 42207, pp. 63-72.

[8] Rannow, M.B., Tu, H.C., Li, P.Y. and Chase, T.R., 2006, January. "Software enabled variable displacement pumps: experimental studies," ASME International Mechanical Engineering Congress and Exposition, Chicago, Illinois, USA, November 5-10, Vol. 47713, pp. 67-76.

[9] Yuan, C., Mao Lung, V.L., Plummer, A. and Pan, M., 2020, "Theoretical and Experimental Studies of a Digital Flow Booster Operating at High Pressures and Flow Rates," *Processes*, 8(2), p. 211.

[10] Pan, M., Johnston, N., Plummer, A., Kudzma, S. and Hillis, A., 2014, "Theoretical and experimental studies of a switched inertance hydraulic system," *Proceedings of the Institution of Mechanical Engineers, Part I: Journal of Systems and Control Engineering*, 228(1), pp. 12-25.

[11] Kogler, H., and Scheidl, R., 2008, "Two basic concepts of hydraulic switching converters," The First Workshop on Digital Fluid Power, Tampere, Finland, October 3, pp.7-30.

[12] Guglielmino, E., Semini, C., Yang, Y. S., Caldwell, D., Kogler, H., and Scheidl, R., 2009, "Energy efficient fluid power in autonomous legged robotics," ASME Dynamic Systems and Control Conference, Vol. 48937, pp. 847-854.

[13] Kogler, H., Scheidl, R., Ehrentraut, M., Guglielmino, E., Semini, C., and Caldwell, D. G., 2010, "A compact hydraulic switching converter for robotic applications," Proceedings of Fluid Power and Motion Control, Bath, UK, September 15–17, pp. 55–66.

[14] Kogler, H. and Scheidl, R., 2010, "Hydraulic switching control of resonant drives," Proceedings of the 12th Mechatronics Forum Biennial International Conference, Zurich, Switzerland, June 28–30, pp. 28–30.

[15] Peng, S., Kogler, H., Guglielmino, E., Scheidl, R., Branson, D.T. and Caldwell, D.G., 2013, "The use of a hydraulic DC-DC converter in the actuation of a robotic leg," IEEE/RSJ International Conference on Intelligent Robots and Systems, Tokyo, Japan, November 3–7, pp. 5859–5864.

[16] Holl, E., Scheidl, R. and Eshkabilov, S., 2017, "Simulation study of a digital hydraulic drive for a knee joint exoskeleton," , Proceedings of the BATH/ASME 2017 Symposium on Fluid Power and Motion Control, Florida, USA, October 16-19, 2017, Paper No. FPMC-4220.

[17] Scheidl, R. and Mittlböck, S., 2018, "A mathematical analysis of a hydraulic binary counter for hydraulic exoskeleton actuation," *International Journal of Hydromechatronics*, 1(2), pp.153-171.

[18] Scheidl, R., Poltschak, F. and Rafetseder, D., 2018, "Hydraulic actuation of exoskeletons–state of the art and prospects," *International Robotics & Automation Journal*, 4(1), p.00096.

[19] Scheidl, R. and Mittlböck, S., 2018, "A hydraulic piloting concept of a digital cylinder drive for exoskeletons," Proceedings of the BATH/ASME 2018 Symposium on Fluid Power and Motion Control, Bath, UK, September 12-14, 2018, Paper No. FPMC2018-8875.

[20] Wang, P., Kudzma, S., Johnston, N., Plummer, A., and Hillis, A., 2011, "The influence of wave effects on digital

switching valve performance," The Fourth Workshop on Digital Fluid Power, Austrian Center of Competence in Mechatronics, Linz, Austria, Sept. 21–22, pp. 10–25.

[21] Pan, M., Johnston, N., Plummer, A., Kudzma, S., and Hillis, A., 2014, "Theoretical and experimental studies of a switched inertance hydraulic system including switching transition dynamics, non-linearity and leakage," *Proceedings of the Institution of Mechanical Engineers, Part I: Journal of Systems and Control Engineering*, 228(10), pp. 802-815.

[22] Pan, M., Johnston, N., Robertson, J., Plummer, A., Hillis, A., and Yang, H. Y., 2015, "Experimental investigation of a switched inertance hydraulic system with a high-speed rotary valve," *Journal of Dynamic Systems Measurement and Control*, 137(12), p. 121003.

[23] Krus, P., Weddfelt, K. and Palmberg, J.O., 1994, "Fast pipeline models for simulation of hydraulic systems," *Journal of Dynamic Systems Measurement and Control*, 116(1), pp. 132-136.

[24] Johnston, N., 2012, "The transmission line method for modelling laminar flow of liquid in pipelines," *Proceedings of the Institution of Mechanical Engineers, Part I: Journal of Systems and Control Engineering*, 226(5), pp. 586-597.